Available online at www.sciencedirect.com
ScienceDirect
International Journal of Solids and Structures 44 (2007) 3076–3099
INTERNATIONAL JOURNAL OF SOLIDS and STRUCTURES
www.elsevier.com/locate/ijsolstr

Twisting of a high authority morphing structure

J. Wang *, A. Nausieda, S.L. dos Santos e Lucato, A.G. Evans

Materials Department, University of California at Santa Barbara, CA 93106, USA

Received 24 September 2005; received in revised form 6 September 2006; accepted 7 September 2006
Available online 16 September 2006

Abstract

A high authority shape morphing plate is examined. The design incorporates an active Kagome back-plane capable of changing the shape of a solid face by transmitting loads through a tetrahedral core. This design is known to perform effectively upon hinging. This article examines limitations on its authority when twisting is required to attain the desired shapes. The specific objective is to ascertain designs that provide the maximum edge twist subject to specified passive load. Non-linear effects, such as face wrinkling, have been probed by using a finite element method and the fidelity of the results assessed through comparison with measurements. The numerical results have been used to validate a dimensional analysis of trends in the actuation resistance of the structure with geometry, as well as the passive load capacity. The forces determined by such analysis have been combined with the failure mechanisms for all subsystems to establish the constraints. The important domains have been visualized using mechanism maps. An optimization has been used to generate load capacity maps that guide geometric design and provide actuator capacity requirements.

Keywords: Shape Morphing; Kagome; Actuators; Optimization; Mechanism Maps

1. Introduction

A class of high authority shape morphing plate structure has been identified and partially characterized (Lu et al., 2001; Hutchinson et al., 2003; Hyun and Torquato, 2002; Christensen, 2000; Wicks, 2003; dos Santos e Lucato and Evans, 2006; dos Santos e Lucato et al., 2005; dos Santos e Lucato et al., 2004). One manifestation is the Kagome structure that can be actuated into relatively intricate surface shapes because of its unique combination of low actuation resistance and high passive strength (Hutchinson et al., 2003; Hyun and Torquato, 2002; dos Santos e Lucato and Evans, 2006; Symons et al., 2005a; Symons et al., 2005b;). The basic design consists of a solid face sheet with an active Kagome back-plane and a tetrahedral core (Fig. 1). In order to induce hinging and twisting, specific members in the Kagome-plane are replaced by linear actuators. When

* Corresponding author. Tel.: +1 805 8935871; fax: +1 805 8938486.
E-mail address: juwang@engineering.ucsb.edu (J. Wang).

0020-7683/$ - see front matter
doi:10.1016/j.ijsolstr.2006.09.008

Nomenclature

d	thickness of Kagome and core members
d_{f}	thickness of solid face sheet
d_{fw}	minimum face thickness to suppress face wrinkling
d_{sm}	stiffness matched face thickness
E	Young's modulus of the material
f_{Tot}	total force on actuators caused by the actuation resistance of the structure plus the passive load
F^*	force induced by actuation resistance of structure
F^*_{Act}	maximum force exerted on the most heavily loaded actuator by the twisting structure
F^*_R	maximum force on the core or Kagome members induced by actuation resistance of structure
F^*_{c}	force on the core members induced by actuation
F^*_{K}	force on the Kagome members induced by actuation
H_{c}	height of the core ($H_{\mathrm{c}} = \sqrt{2/3}L$)
J	Work done by actuators
J_{c}	strain energy stored in core when actuated
J_{f}	strain energy stored in solid face when actuated
J_{K}	strain energy stored in Kagome when actuated
L	length of Kagome and core members
m	mass of the structure
P	passive external load
$\overline{P}$	specific load capacity of the structure ($\overline{P} = P_{\max}/m$)
$P_{\max}$	maximum achievable external load
s	span of the structure
w	width of the structure
X_{Act}	load capacity of actuator
$\mathfrak{I}$	forces induced by external load
$\mathfrak{I}_{\mathrm{c}}$	force on core members
$\mathfrak{I}_{\mathrm{Act}}$	force on actuators
γ	twist angle ($\gamma = 2\Delta/w$)
ε_Y	yield strain of the material
ρ	density of the material
$\bar{\sigma}_{\mathrm{f}}$	stress in solid face induced by actuation
σ_{f}	stress in solid face due to external load
σ_{K}	stress in Kagome due to external load
σ_{N}	nominal stress in the Kagome back-plane induced by external load
σ_{truss}	stress on a Kagome truss member
σ_Y	yield stress of the material
Δ	edge displacement attained upon twisting.
$\Delta_{\max}$	maximum achievable twist displacement subject to specified X_{Act} in the absence of an external load
Π_{Act}	critical value of external load to cease actuator function
Π_{CB}	critical external load at which the core buckles
Π_{CY}	critical external load at which the core yields
Π_{FB}	critical external load at which the face buckles
Π_{FY}	critical external load at which the face yields
Π_{KB}	critical external load at which the Kagome buckles
Π_{KY}	critical external load at which the Kagome yields

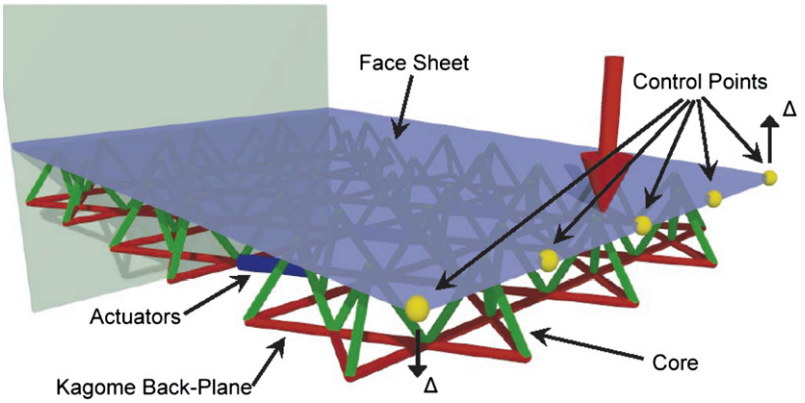

Fig. 1. Schematic representation of the Kagome demonstration structure. The solid face is shown in blue, the core in green and the Kagome back-plane in red. Actuators are placed in-lieu of the Kagome-members. The control points are used to define the target deformation. (For interpretation of the references to color in this figure legend, the reader is referred to the web version of this article.)

the system must interface with an external environment, such as a pressure load on the surface of an aerospace vehicle, the design with one solid face supported by a Kagome back plane and a core is required. The authority of the structure (product of load supported and displacement) has been examined in the hinging mode, with accompanying experimental validation (dos Santos e Lucato et al., 2004). This assessment has included the placement of the actuators and the preferred materials. Many of the desired shape changes can be achieved by hinging along the three equivalent directions provided by the structure (Fig. 1). Nevertheless, twisting is indispensable in some instances. Since this structure performs differently in twisting than in hinging, the primary objective of this article is to establish the limitations on performance that arise when twisting is required.

A preliminary examination of twisting displacements has been conducted by using a linear formulation of the induced forces (dos Santos e Lucato et al., 2005). This investigation used a genetic algorithm to ascertain the placement of the actuators. It focused on the demonstration structure depicted in Fig. 1. It ascertained the largest displacements that can be realized subject to the avoidance of structural failure by either buckling or yielding of either the truss members or the solid face, within the load capacity of representative actuators. It remains to verify these characteristics by pursuing a more detailed numerical analysis, accompanied by the design and conduct of critical experiments. In this article, such an assessment is performed on the same demonstration structure, followed by a generalization that illustrates trends with materials and dimensions.

The article is organized in the following manner. The features of the demonstration structure are described, as well as the actuator placements. Preliminary calculations are used to probe the practical limit on the achievable twisting: due to yielding, buckling and face wrinkling. Numerical parameter studies are used to find trends in displacement and to ascertain designs that inhibit the undesirable responses. The trends are used for optimization.

2. Structure

The basic structure (Fig. 1) comprises a solid face, a Kagome active-plane and tetrahedral core. It is actuated in a manner that causes the free end to rotate, such that the edges displace in the vertical direction, by Δ, resulting in a twist angle, $\gamma = 2\Delta/w$, where w is the panel width. Based on the preference for Ti alloys elucidated in a previous study (dos Santos e Lucato and Evans, 2006), most of the assessments are made using Ti–6Al–4V as the material of choice. However, because of fabrication limitations, the experimental assessment uses a combination of a high strength Al alloy (6061-T6) face with a truss system made from 304 stainless steel. To achieve the target shapes, some members of the Kagome are replaced by linear stepper motors (or turnbuckles). The structure may be fully or partially patched to gain

structural capability, as described elsewhere (Symons et al., 2005a) and summarized in Appendix A (Fig. A.1). To illustrate the characteristics, a specific demonstration structure has been selected (Fig. 1). However, the methods are sufficiently general that the results could be readily extended to panels with a larger number of units.

The demonstration panel is partially-patched (Appendix A). It includes 6 hexagonal units of the Kagome in the longitudinal dimension and 4 for the width. Since the failure modes are affected by the slenderness of the members (length to diameter, L/d) (Hutchinson et al., 2003), two different choices have been made: one limited by buckling ($L/d = 33$) and the other by yield or fatigue ($L/d = 20$). The truss lengths, L, have been chosen to accommodate commercially available linear stepper motors: $L = 5.1$ cm (dos Santos e Lucato et al., 2004). The face thickness, d_f, has been chosen with the expectation that minimum weight designs arise when the face is stiffness matched to the Kagome plane, $d_f = d_{sm}$ (Christensen, 2000). In practice, the choices are constrained by the thickness of commercially available sheet materials.

Two placement schemes are used, assuming 8 actuators in both cases.

(i) For benchmarking of the response, an entire row at the center of the plate is replaced by actuators (Fig. 2a). These locations are globally sub-optimal from the perspective of the edge twist (dos Santos e Lucato et al., 2005). However, the overall shape may be more desirable in some circumstances, as discussed below.

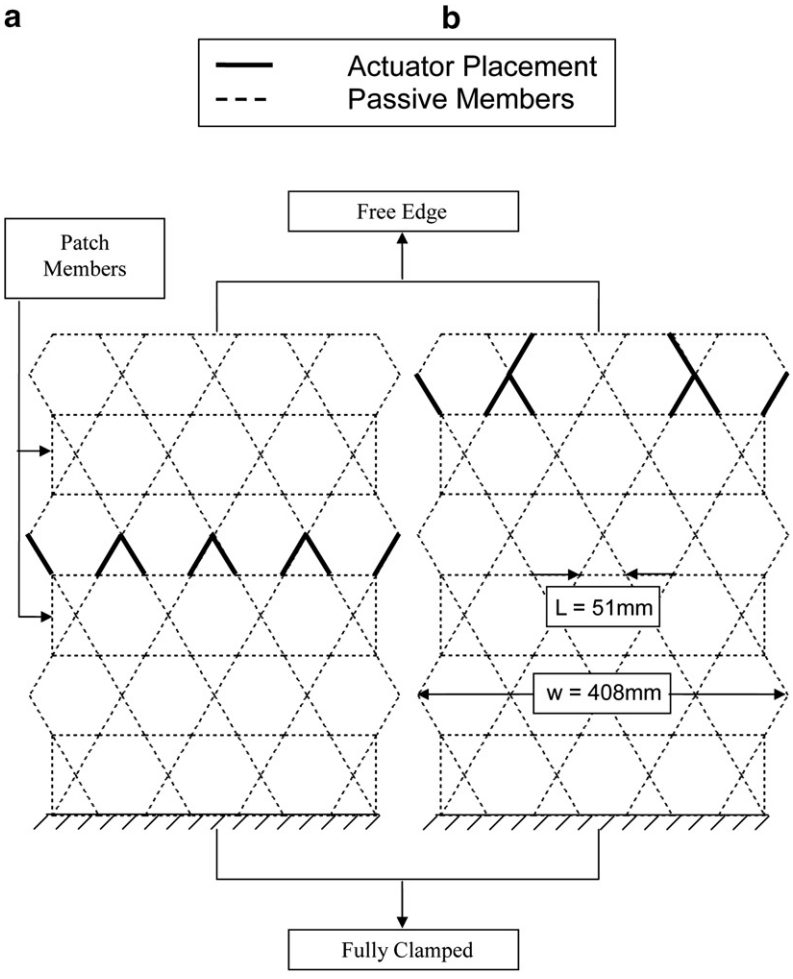

Fig. 2. Two different placement schemes of the actuators: (a) linear (sub-optimal for an edge twist perspective); (b) optimal.

(ii) To assess the best possible edge twist response, the actuators are placed at the optimal location suggested by a previous assessment (dos Santos e Lucato et al., 2005) (Fig. 2b).

3. Definitions of forces and loads

The analysis involves forces and stress associated with an external load imposed on the free-end, as well as those induced by the actuation. To distinguish these contributions, the salient entities are defined in this section. Moreover, critical values of the imposed load at which failure occurs by one of the operative mechanisms (buckling, yielding, wrinkling, actuator cessation) are also defined.

Forces and stresses due to external load. This load induces forces and stresses in the members and on the actuators. The *forces* are designated using the symbol, $\Im : \Im_{\mathrm{Act}}$ on the actuators and $\Im_{\mathrm{c}}$ on the core members. The maximum *stresses* induced are σ_{K} on the Kagome members and σ_{f} in the face sheet.

Forces and stresses due to the actuation resistance of the structure. The forces are designated using the symbol, F^*: those on the actuators are F^*_{Act}, on the core members F^*_{c} and on the Kagome members, F^*_{K}. The stress induced in the face sheet is $\bar{\sigma}_{\mathrm{f}}$. Because of the various failure mechanisms that operate in response to these forces, there is a maximum load, $P_{\max}$, that can be supported when the structure is actuated to a prescribed twist angle, γ. This maximum is ascertained by identifying the first subsystem to fail.

The critical loads for subsystem failure are designated using the symbol, Π. These include the load at which the actuator ceases to function, Π_{Act}, the loads at which the core and Kagome members and the face buckle, Π_{CB}, Π_{KB}, Π_{FB}, as well as the loads at which these constituents yield, Π_{CY}, Π_{KY}, Π_{FY}. Note that the various Π quantities represent the *imposed loads* at which one of the failure mechanisms operates.

The total force on the actuators, f_{Tot}, is the sum of the contributions from the actuation resistance of the structure and the passive load. The critical value of this force at which the actuators cease to operate is designated, X_{Act}. In all cases, proportional actuation is assumed and solutions are obtained by seeking that actuator in the ensemble that first attains X_{Act}.

4. Numerical procedures

The calculations are conducted using a finite element method with the commercial code ABAQUS. To simulate the complete actuation system, the core and Kagome members are modeled using linear Timoshenko-type beams, while the solid face sheet is discretized using general-purpose quadrilateral shell elements. A total of 10 beam elements are used per member to capture bending and buckling. The actuators are incorporated into the model by means of truss elements, with representative cross-sectional area. Actuation is achieved by thermal expansion of these truss elements. One side of the structure is fully clamped, while the other is free to displace.

As in prior assessments (dos Santos e Lucato et al., 2004), linear elastic analysis is used to ascertain the actuation resistance as well as the effects of the passive load. The ensuing structural determination is conducted by comparing the loads and stresses with failure criteria based on buckling and yielding. The calculations are conducted for two circumstances.

(a) An optimization routine is used to assess the maximum twist displacements for specified actuator load capacity (dos Santos e Lucato et al., 2004). The method also determines the ratios of the strains required in the actuators.
(b) To characterize the failure modes, such as face wrinkling and buckling of the Kagome and core members, a large-displacement method that allows geometric non-linearity is used. It generates wrinkling patterns amenable to comparison with experimental observations.

The latter is used to assess the response to the passive load and to determine the resistance of the structure to twisting.

Table 1
Maximum twist displacements obtained for different assemblies and the strains in the actuators to realize them, subject to an actuator load capacity, X_{Act}, 40 N

Assembly (face/core/Kagome)	Truss thickness d (mm)	Face thickness d_f (mm)	Maximum twist Δ_{max} (mm)	Actuation strains in the 8 actuators
Al AlIoy/SS/SS	1.52	0.152	4.6	{−0.049, −0.0016, −0.017, 0.0065, −0.0065, 0.017, 0.0016, 0.049}
Ti/Ti/Ti	1.52	0.132	7.8	{−0.080, −0.0019, −0.028, 0.011, −0.011, 0.028, 0.0019, 0.080}

5. Initial assessment

Preliminary calculations have been used to gain insight into responses that limit the achievable twisting. The emphasis has been on the linear actuator configuration, which exacerbates the detrimental responses. The ranges of the actuation strains needed to realize large displacements, while maintaining the straightness of the edge (Fig. 1), have been estimated using linear analysis (both material and geometric), subject to a maximum allowable force on the actuators, X_{Act} (Table 1). Thereafter, the consequences of imposing these strains are determined by using linear elasticity (yielding suppressed) but allowing geometric non-linearity. This analysis is performed without imperfections because the structure (even when partially-patched) is relatively imperfection insensitive (Appendix A).

Upon imposing the strains, the demonstration panel is found to exhibit appreciable *face wrinkling* (Fig. 3). The implication is that this undesirable feature must be suppressed by thickening the face, even though the accompanying increase in actuation resistance must diminish the realizable twisting. The goal will be to find the minimum face thickness needed to achieve the required displacement while avoiding face wrinkling. This thickness is denoted, d_{fw}.

An assessment of the elastic energy stored in the three sub-elements of the structure (core, face and Kagome), summarized in Table 2, indicates that the resistance to actuation is provided almost equally by the face sheet, core members and Kagome plane. This feature differs markedly from that for hinging (dos Santos e Lucato et al., 2004), wherein essentially all of the resistance is provided by the core members located above the actuators (Table 2). The deformation of the Kagome members calculated at maximum twist (Fig. 4) affirms that they experience bending. This characteristic provides some appreciation for the trends in achievable twisting with the relative dimensions of the truss members and the face, discussed next.

6. Actuation resistance

Calculations have been performed for the all Ti-alloy system, in which the face thickness has been varied systematically for two values of the truss slenderness ($L/d = 20$ and 33), and two disparate values of the actuator capacity, $X_{Act} = 40$ N and $X_{Act} = 400$ N. The calculations have been conducted in the absence of a passive load. An optimization routine is used to ascertain the maximum twist displacements, Δ_{max}, that can be achieved subject to the specified actuator capacity, X_{Act}. The procedure is described briefly in Appendix II. A detailed description can be found in dos Santos e Lucato et al. (2004)). Results have been obtained for both actuator placements. The displacements attained are plotted as a function of face thickness in Fig. 5. For the linear placement (Fig. 5a) the displacements extend over a sufficiently wide range that a logarithmic coordinate is used. Whereas, for the optimal placement, linear coordinates suffice (Fig. 5b).

Major effects of X_{Act} and L/d on Δ_{max} are evident. Note that, as expected, much larger displacements can be realized when the actuators are placed in the optimal configuration rather than linear. Examples of the associated deformations are illustrated in Fig. 6, revealing the combinations susceptible to wrinkling. The latter allows d_{fw} to be ascertained and superposed on the displacements (Fig. 5). The fidelity of these results is assessed by experimental measurements described in Appendix III.

To gain insight into aspects of the actuation resistance of the structure, the elastic energies stored within the Kagome members and the face have been calculated and normalized by the work done by the actuators, J. A

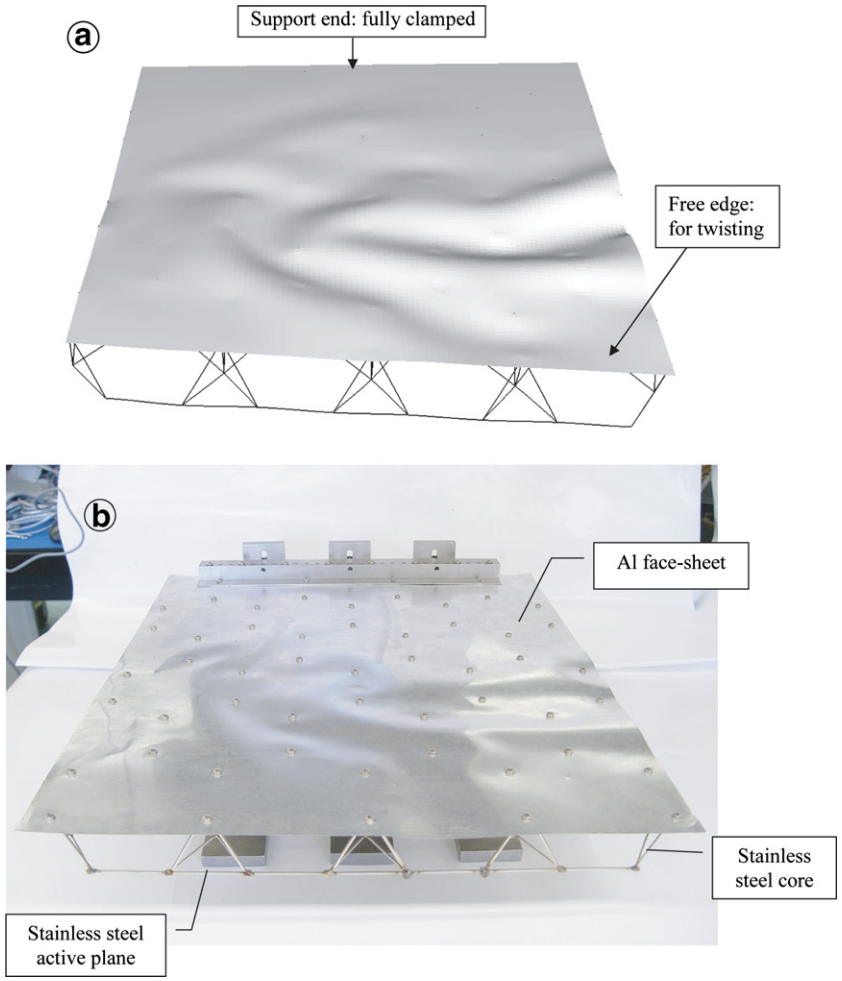

Fig. 3. Wrinkling in the solid face upon actuation. This assembly has Al alloy face with stainless steel core and Kagome back-plane: (a) finite element simulation; (b) experimental result.

Table 2
Elastic energy stored in the sub-systems for hinging and twisting with actuators at linear arrangement. The assembly is the demonstration structure

		Face sheet	Core	Kagome back-plane
Strain energy	Twisting	4.1×10^{-2}	2.8×10^{-2}	3.6×10^{-2}
	Hinging	2.3×10^{-4}	1.1×10^{-2}	1.3×10^{-7}

The energy is in Joules.

synopsis of the results for two different actuator capacities (40 and 400 N) over a wide range of face thickness is presented in 7. The results refer to the linear actuator placement (Fig. 7a) and the optimal placement (Fig. 7b). Lines have been placed through the calculated results to indicate the trends. Several characteristics are apparent. (i) At specified face thickness, the results affirm that the normalized strain energies are the same for both actuator capacities. (ii) Differing trends with face thickness are apparent for the two actuator placements. This difference is attributed to the differing shapes induced in the face (see Fig. 6). Briefly, for the linear configuration (Fig. 7a) most of the energy is stored in the Kagome plane, due to member bending (see Fig. 4). The contribution from the face is smaller. For the optimal placement (Fig. 7b), when the faces are thick, the energy is dominated by the face stretching needed to realize the deformation pattern (Fig. 6). This contribution

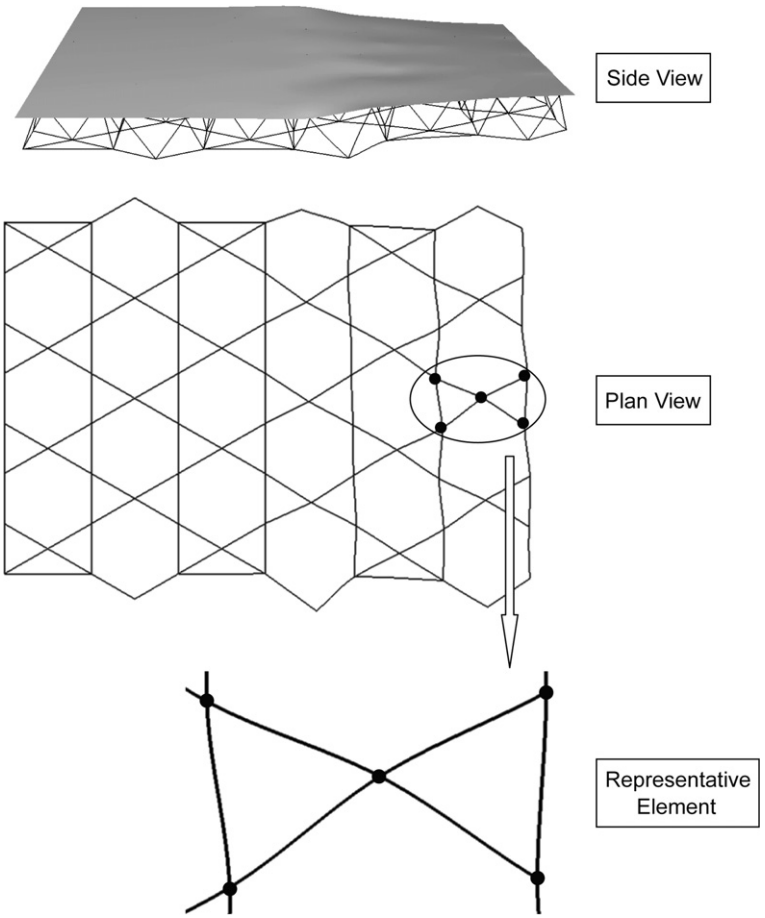

Fig. 4. The bending of the Kagome members when the structure with linear actuators is twisted (Deformation scale factor is 7): this assembly has Al alloy face ($d_f = 0.3$ mm) with stainless steel core and Kagome back-plane. The actuation strains in the 8 actuators are $\{-0.048, -0.0014, -0.017, 0.0064, -0.0064, 0.017, 0.0014, 0.048\}$. The maximum twist displacement is 4.6 mm.

decreases dramatically for thinner faces, as the stretching energy diminishes. (iii) The variations in stored energy with face thickness are not monotonic. Numerical error is believed responsible because, for each face thickness, it was required that estimates of the optimal actuation strains be obtained using the procedure described by dos Santos e Lucato et al. (2005). The associated approximations result in some variability between nominally similar calculations.

The twist displacements, Δ_{max}, realizable at a face thickness where wrinkling is excluded (that is, for situations where the response is geometrically-linear) can be unified by invoking results ascertained from the previous hinging investigation, which provided the salient non-dimensional groups for bending and stretching (dos Santos e Lucato et al., 2004). It is recalled that the actuation resistance is the force induced in the actuators upon actuation. For a material with Young's modulus, E, the resistance to actuation caused by bending in the core and Kagome members scales as:

$$\frac{F^*_{Act}}{\Delta_{max} EL} \sim \left[\frac{d}{L}\right]^4 \tag{1a}$$

The analogous scaling for face stretching is:

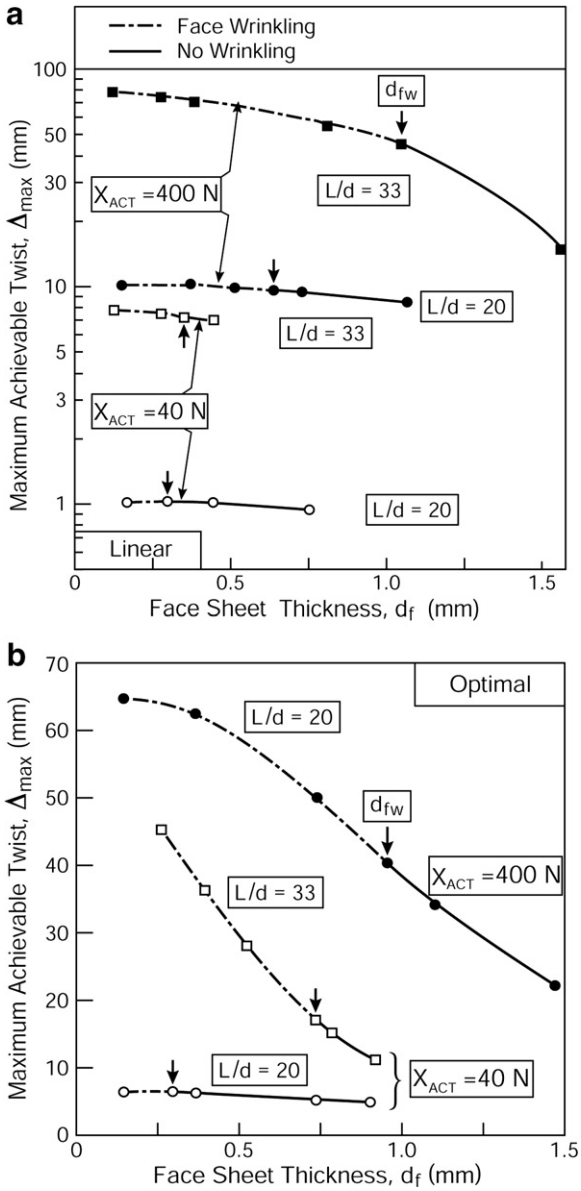

Fig. 5. Maximum achievable twisting displacements attained for two different aspect ratios ($L/d = 20$, 33) and two different values of the actuator capacity ($X_{\mathrm{Act}} = 40$ N, 400 N): (a) linear placement of the actuators; (b) optimal placement of the actuators. The vertical arrows indicate the face wrinkling transitions at, d_{fw}. The results are obtained without an external load.

$$\frac{F^*_{\mathrm{Act}}}{\Delta_{\max} EL} \sim \left[\frac{d_{\mathrm{f}}}{L}\right] \tag{1b}$$

In these formulae, F^*_{Act} is the maximum force induced in *the most heavily loaded actuator* by the twisting structure. By assuming that the total force is the sum of the resistances caused by member bending and face stretching then:

$$\frac{F^*_{\mathrm{Act}}}{EL\Delta_{\max}} = A_a\left(\frac{d}{L}\right)^4 + B_a\left(\frac{d_{\mathrm{f}}}{L}\right) \tag{1c}$$

where A_a and B_a are quantities to be obtained by fitting to the finite element results.

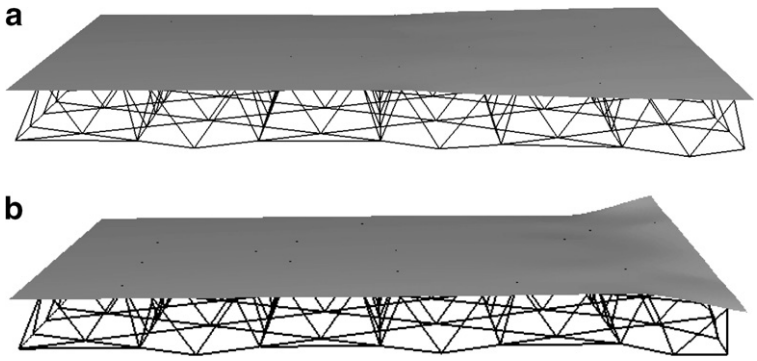

Fig. 6. Deformations upon maximum twist for the two different actuator placements ($L/d = 33$, $X_{\mathrm{Act}} = 40$ N, $d_{\mathrm{f}} = d_{\mathrm{fw}}$): (a) linear placement; (b) optimal placement.

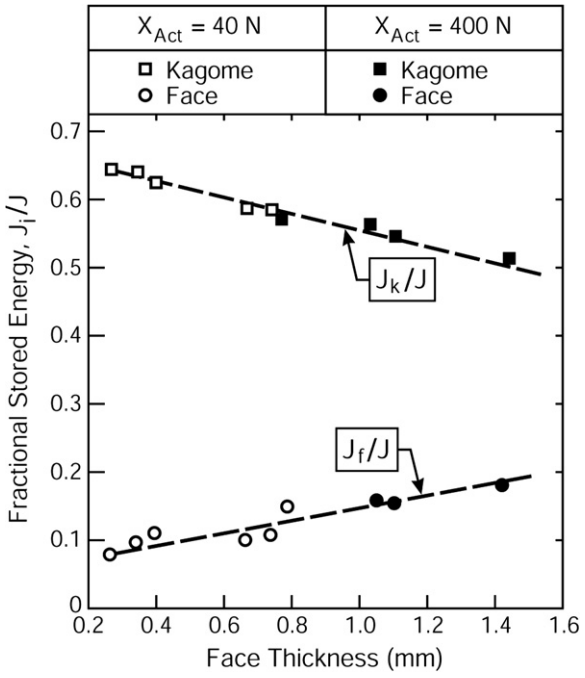

Fig. 7(a). Elastic energy stored in the Kagome back-plane and solid face sheet for the linear actuator placement. Note that most energy is stored in the Kagome plane due to member bending. The symbols give the actual results. The lines are used to highlight the trends.

To assess the merits, the numerical results are plotted using these non-dimensional parameters (Fig. 8). Note that by using d_{f}/L as the abscissa and fixing d/L, each fit to (1c) is a straight line. The correspondence evident in the Figure signifies that (1) has sufficient fidelity for present purposes. The fit for the linear actuator configuration gives (Table 3): $A_a = 1.0$, $B_a = 2.3 \times 10^{-4}$. The corresponding results for the optimal configuration are: $A_a = 0.16$, $B_a = 6.6 \times 10^{-5}$. These magnitudes affirm the large (order of magnitude) reduction in the resistance when the actuators are optimally placed for edge twist. They also reveal that, for the latter, face stretching becomes the dominant contribution to the resistance, especially when the face is thick enough to avoid wrinkling. This effect accounts for the trend in stored energy with face thickness (Fig. 7b) and the linear downward trend in achievable twist displacement as the face thickens (Fig. 5).

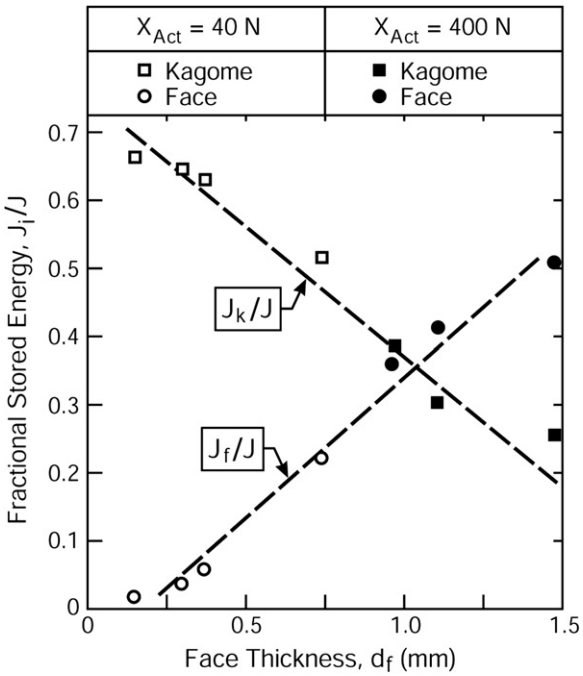

Fig. 7(b). Elastic energy stored in the Kagome back-plane and solid face sheet for the optimal actuator placement. Most of the energy is either in the Kagome plane, due to member bending (small face thickness) or in the face (large face thickness), due to face stretching. The symbols give the actual results. The lines are used to highlight the trends.

7. Forces in the structure induced by actuation

The forces and stresses induced in the different subsystems of the structure upon actuation have been ascertained from the preceding numerical results. The largest forces induced on the members of the subsystems, F_R^*, satisfy:

$$\frac{F_R^*}{EL\Delta_{\max}} = A_R\left(\frac{d}{L}\right)^4 + B_R\left(\frac{d_f}{L}\right) \tag{2a}$$

The magnitudes of the coefficients (A_R, B_R) for each of the subsystems are summarized in Table 2. Within each category (linear or optimal), one set of results refers to the maximum compressive force, pertinent to failure by buckling. The other refers to the maximum absolute value of the force (whether tension or compression), used to ascertain the incidence of yielding. An example of the correspondence between (2a) and the detailed numerical calculations is demonstrated in Fig. 9: (a) refers to the forces on the Kagome members for the linear actuator arrangement and (b) to that on the core members in the optimal actuator placement.

The corresponding result for the average stresses induced in the faces between neighboring core supports is:

$$\frac{\bar{\sigma}_f L}{E\Delta_{\max}} = C_f\left(\frac{d}{L}\right)^4 + D_f\left(\frac{d_f}{L}\right) \tag{2b}$$

The coefficients are given in Table 3.

8. Forces and stresses induced by the passive load

The passive loads that can be sustained without failure have been derived by assuming a cantilever plate, span s, and width w, subject to a line load (total load), P (Ashby et al., 2000), imposed at the free end of the panel. This load induces a force $\Im_{Act}$ on the actuators: (dos Santos e Lucato et al., 2004)

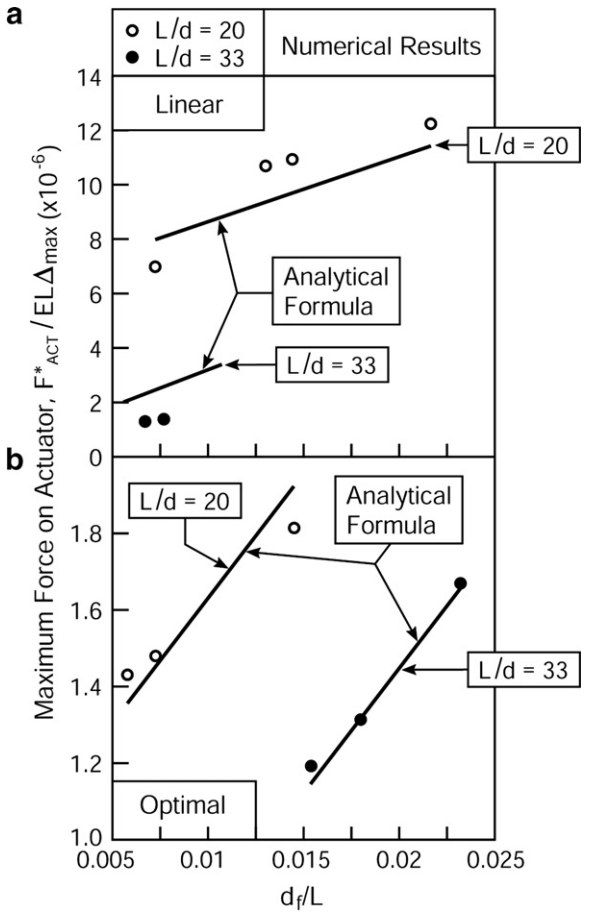

Fig. 8. The forces induced by the structure on the actuators: a comparison of results ascertained numerically (symbols) and the analytic formulae (lines): (a) actuators in a linear arrangement; (b) actuators in optimal placement. The analytical formulae are linear in the coordinate system since each line is plotted with fixed d/L.

$$\mathfrak{I}_{\mathrm{Act}} = \Theta \frac{s}{w} P \tag{3}$$

The coefficient Θ differs for the two actuator placements: $\Theta_{\mathrm{c}} = 0.58\sqrt{3/2}$ for linear and $\Theta_o = 0.58\sqrt{1/6}$ for optimal (Hutchinson et al., 2003). The nominal stress induced in the Kagome back-plane is related to the bending moment, $M = Ps$, by

$$\sigma_{\mathrm{N}} = \sqrt{\frac{3}{2}} \frac{Ps}{dwL} \tag{4a}$$

Recall that the member length, L, is related to the core height by, $L = \sqrt{3/2} H_{\mathrm{c}}$ (dos Santos e Lucato et al., 2004). This stress is related to the actual stress on a truss member σ_{truss} by

$$\begin{aligned} \sigma_{\mathrm{N}} &= -\sqrt{3} \frac{d}{L} \sigma_{\mathrm{truss}} \quad (\text{truss member } X) \\ \sigma_{\mathrm{N}} &= \frac{\sqrt{3}}{2} \frac{d}{L} \sigma_{\mathrm{truss}} \quad (\text{truss member } Y) \end{aligned} \tag{4b}$$

where trusses X are parallel to the width and Y at $\pm 30°$ to the span. The maximum stress in the Kagome trusses is thus

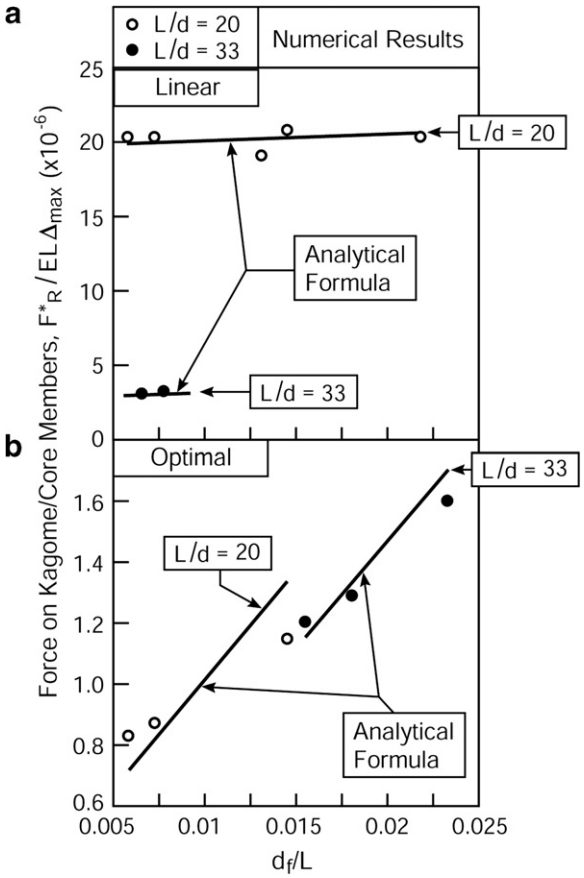

Fig. 9. The forces induced by the structure: a comparison of results ascertained numerically (symbols) and the analytic formulae (lines): (a) the forces on the Kagome members when the actuators are located in a linear arrangement; (b) the forces on the core members when the actuators are in the optimal placement.

Table 3
The coefficients for the numerically fitted equations defining the maximum forces or stresses induced in the actuators and sub-systems by actuation

Numerical coefficients	Linear configuration	Optimal configuration
A_a	1.0	0.16
B_a	2.3×10^{-4}	6.6×10^{-5}
(A_K) Compressive	3.2	0.17
(B_K) Compressive	4.6×10^{-5}	6.1×10^{-5}
A_K	3.2	0.18
B_K	1.2×10^{-4}	6.1×10^{-5}
(A_c) Compressive	2.1	4.8×10^{-2}
(B_c) Compressive	7.8×10^{-3}	7.2×10^{-5}
A_c	2.1	4.8×10^{-2}
B_c	8.7×10^{-3}	7.6×10^{-5}
(C_f) Compressive	215	30
(D_f) Compressive	-1.6×10^{-3}	4.1×10^{-2}
C_f	2.9×10^{-3}	150
D_f	−0.23	0.22

A_a and B_a are the coefficients in (1c) for the force in the actuators. A_K, $B_K A_c$ and B_c are the coefficients A_R and B_R in (2a), where the subscripts K and c denote Kagome and core, respectively). C_f and D_f are the coefficients in 2(b) for the stress in the face sheet.

$$\sigma_{\mathrm{K}} = \sqrt{2}\frac{Ps}{d^2 w} \tag{4c}$$

The corresponding maximum stress in the face sheets and the maximum force in the core members are related to the bending moment and the core height, respectively, by (Wicks and Hutchinson, 2001)

$$\sigma_{\mathrm{f}} = \frac{Ps}{d_{\mathrm{f}} w H_{\mathrm{c}}} \tag{5a}$$

and

$$\Im_{\mathrm{c}} = \frac{\sqrt{3}PL\sqrt{L^2 - H_{\mathrm{c}}^2}}{wH_{\mathrm{c}}} \tag{5b}$$

9. Mechanism maps

To derive mechanism maps, the preceding results obtained using linear elasticity (no yielding) and geometric linearity (no wrinkling and no buckling) are used. Accordingly, the forces induced in the actuators due to the twisting resistance of the structure plus those from the passive load are additive. In that case, the total force becomes:

$$f_{\mathrm{Tot}} = \Im_{\mathrm{Act}} + F^*_{\mathrm{Act}} \tag{6}$$

Recall that the force induced by the passive load is derived by assuming a cantilever plate (Ashby et al., 2000), wherein only the geometry of the structure and the magnitude of the passive force are involved. By equating f_{Tot} with the load capacity of the actuator, X_{Act}, the critical external load that causes the actuators to cease operation can be ascertained as:

$$\Pi_{\mathrm{Act}} = \frac{w\Delta_{\max}L}{\Theta s}E\left\{\frac{X_{\mathrm{Act}}}{E\Delta_{\max}L} - \left[A_a\left(\frac{d}{L}\right)^4 + B_a\left(\frac{d_{\mathrm{f}}}{L}\right)\right]\right\} \tag{7}$$

The forces induced in the subsystems are also additive. They lead to the following constraints.

The critical values of the passive load at which failure occurs *by yielding* (at strain, ε_Y) are: *for the Kagome members*,

$$\Pi_{KY} = \frac{wd^2}{\sqrt{2}s}E\left\{\varepsilon_Y - \frac{L\Delta_{\max}}{d^2}\left[A_{\mathrm{K}}\left(\frac{d}{L}\right)^4 + B_{\mathrm{K}}\left(\frac{d_{\mathrm{f}}}{L}\right)\right]\right\} \tag{8a}$$

for the core members:

$$\Pi_{CY} = \sqrt{\frac{2}{3}}\frac{wd^2}{L}E\left\{\varepsilon_Y - \frac{L\Delta_{\max}}{d^2}\left[A_{\mathrm{c}}\left(\frac{d}{L}\right)^4 + B_{\mathrm{c}}\left(\frac{d_{\mathrm{f}}}{L}\right)\right]\right\} \tag{8b}$$

and for the face:

$$\Pi_{FY} = \sqrt{\frac{2}{3}}\frac{wd_{\mathrm{f}}L}{s}E\left\{\varepsilon_Y - \frac{\Delta_{\max}}{L}\left[C_{\mathrm{f}}\left(\frac{d}{L}\right)^4 + D_{\mathrm{f}}\left(\frac{d_{\mathrm{f}}}{L}\right)\right]\right\} \tag{8c}$$

The corresponding results for *member buckling are: for the Kagome members*

$$\Pi_{KB} = \frac{wd^4}{\sqrt{2}sL^2}E\left\{\frac{\pi^2}{12} - \frac{L^3\Delta_{\max}}{d^4}\left[A_{\mathrm{K}}\left(\frac{d}{L}\right)^4 + B_{\mathrm{K}}\left(\frac{d_{\mathrm{f}}}{L}\right)\right]\right\} \tag{9a}$$

and for *the core members*:

$$\Pi_{CB} = \frac{wd^4}{\sqrt{3}L^3}E\left\{\frac{\pi^2}{4\sqrt{2}} - \sqrt{2}\frac{L^3\Delta_{\max}}{d^4}\left[A_c\left(\frac{d}{L}\right)^4 + B_c\left(\frac{d_f}{L}\right)\right]\right\} \tag{9b}$$

For *face wrinkling*:

$$\Pi_{FB} = \sqrt{\frac{2}{3}}\frac{wd_f^3}{sL}E\left\{\frac{49\pi^2}{144(1-\nu^2)} - \frac{L\Delta_{\max}}{d_f^2}\left[C_f\left(\frac{d}{L}\right)^4 + D_f\left(\frac{d_f}{L}\right)\right]\right\} \tag{10}$$

These results can be used to construct mechanism maps, using procedures described elsewhere (dos Santos e Lucato and Evans, 2006). Detailed results are presented for actuators with optimal placement (Fig. 10 and Table 4). The maps use the face and core member thickness as coordinates. Each map is constructed for a

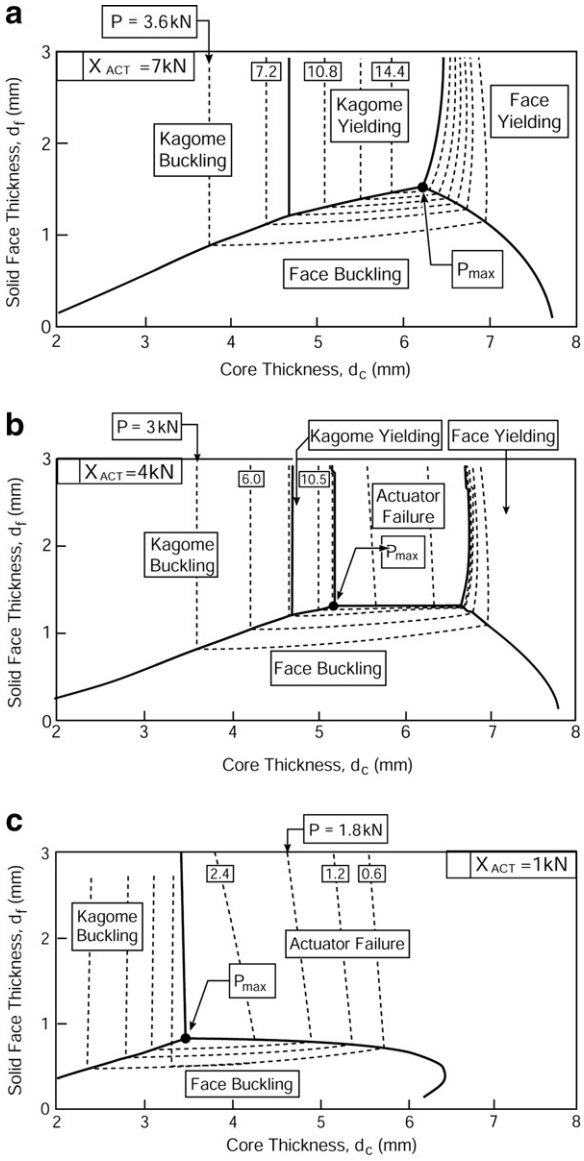

Fig. 10. Mechanism maps and maximum passive loads that can be supported for a twist displacement of 5.1 mm and three actuator capacities: (a) $X_{ACT} = 1$ kN; (b) $X_{ACT} = 4$ kN; (c) $X_{ACT} = 7$ kN.

Table 4
The maximum passive loads and geometric dimensions needed to achieve a twist displacement of 5.1 mm within different actuator capacities

X_{ACT} (kN)	P_{max} (kN)	d (mm)	d_f (mm)
1.0	2.9	3.5	0.85
4.0	11	5.2	1.3
6.3	17	6.3	1.5
7.0	17	6.4	1.6

specified actuator load capacity, X_{Act}. The failure domains are revealed in the maps. The contours indicate the passive loads that can be supported without failure occurring by the designated mechanism.

This exercise reveals three different response modes, dependent on the actuator load capacity, X_{Act}.

(*i*) *High load actuators*, $X_{Act} \geqslant 6$ kN (Fig. 10a). In this case, the loads that can be supported are dictated entirely by structural considerations. The maximum load capacity is at the confluence of three mechanisms: Kagome buckling, face yielding and face buckling.

At lower X_{Act}, the boundaries between the mechanisms represented by this map remain invariant: but a domain of actuator failure enters, becoming more expansive as X_{Act} decreases.

(*ii*) *Intermediate load actuators*, 6 kN $\geqslant X_{Act} \geqslant$ 3 kN (Fig. 10b). The domain of actuator failure is apparent at the center of the map. The maximum is at the confluence of actuator failure, Kagome yielding and face wrinkling.

(*iii*) *Low load actuators*, $X_{Act} \leqslant 3$ kN (Fig. 10c). In this case, actuator failure occupies a large domain and the maximum load capacity is at the confluence of actuator failure, Kagome member buckling and face wrinkling.

These different domains will become apparent when the system is optimized, as discussed next.

10. Optimization

The objective of the optimization is to seek the topology and the actuator capacity that realize a specified twist while supporting the largest possible external load. Ascertaining the maximum requires that the first subsystem to fail be identified by using:

$$P_{max} = \min(\Pi_{KY}, \Pi_{KB}, \Pi_{CY}, \Pi_{CB}, \Pi_{FY}, \Pi_{FB}, \Pi_{Act}) \tag{11}$$

The load capacity at specified mass is typically the important engineering metric. The mass of the structure is (dos Santos e Lucato and Evans, 2006):

$$m = 24\left\{6\left[L - \frac{1}{\sqrt{3}}d\right]d^2\rho + \left[\frac{\sqrt{3}}{2} + 6L\right]d^2\rho + 2\sqrt{3}L^2 d_f\rho\right\} \tag{12}$$

with ρ being the density of the material. The specific load capacity thus becomes: $\overline{P} = P_{max}/m$.

The effect of varying the actuator capacity on $\overline{P}$ is plotted in Fig. 11. Every point represents a non-linear optimization with the specified X_{Act}. Note the three domains anticipated by the mechanism maps. At low actuator capacity, the load capability increases rapidly as the actuators improve because the concomitant increase in the Kagome member stubbiness inhibits buckling. Once the actuators become sufficiently strong, these members transition to failure by yielding, causing a diminished rate of change of $\overline{P}$ with actuator capacity. Finally, when the design becomes structure-limited, X_{Act} has no further effect (the decrease in $\overline{P}$ in Fig. 11 at largest X_{Act} is a consequence of increasing the stubbiness to support stronger actuators, causing the design to translate away from the structural optimum).

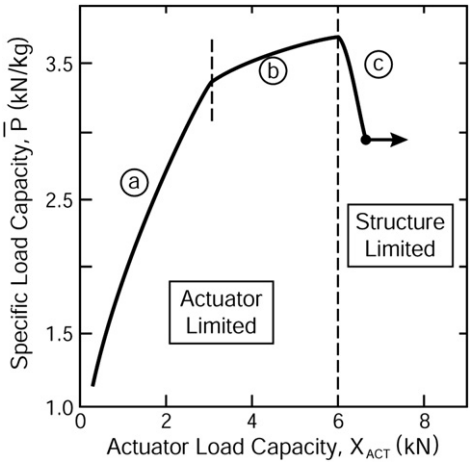

Fig. 11. External specific load capability as function of actuator load capacity (The prescribed twist displacement is 5.1 mm).

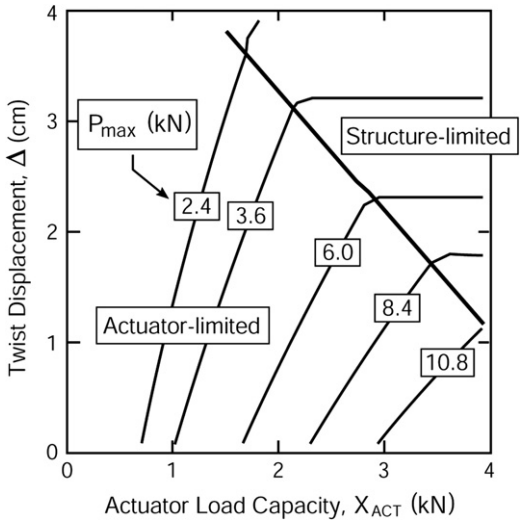

Fig. 12. A map of the maximum load capability as function of actuator capacity and twist displacement.

Since the preceding results are optimal for only one twist displacement ($\Delta = 5.1$ mm), the load capacity for a wide range of displacements has been computed by using a non-linear optimization with Mathematica (Wolfram Research, 2003). The result (Fig. 12) reveals the actuator and structure-limited domains. In the former, $P_{\max}$ increases with X_{Act}. This diagram allows the selection of actuators capable of providing specified levels of edge twist and load capacity.

11. Conclusion

Analytic and numerical assessments have been used to guide and characterize the design of a high authority shape morphing Kagome structure that requires twisting to achieve the desired shapes. Two different actuator placement schemes have been explored. Optimal placement renders the maximum achievable edge twist displacement. A linear placement induces a more gradual shape change but at reduced edge twist.

Non-linear responses of the structure to actuation have been simulated numerically. Trends in the elastic energy stored in the subsystems indicate that face stretching and truss bending are the major contributions to the actuation resistance. Analytic models have been derived for the geometric scaling and their fidelity

established by comparison with numerical results. A large reduction in the resistance when the actuators are optimally placed is consistent with the larger achievable edge twist.

The forces associated with the actuation resistance and those induced by passive loads have been derived and combined with the failure mechanisms to create mechanism maps. These maps reveal that, at low actuator capacity, the optimal design resides at the confluence of the actuator limit and two structural failure mechanisms: while at high actuator capacity, the optimal is at the confluence of three structural failure mechanisms. A design diagram has been constructed that allows determination of the actuator capacity needed to attain specified edge twist while supporting a required load.

Appendix A. Structural assessment of the kagome plane

The passive load capacity of the Kagome plane has been evaluated with emphasis on the role of imperfections. Both partially and fully-patched designs are pursued (Fig. A.1). The patches are used to suppress low strength bending modes that exist in the structure (these modes are equivalent to zero-stiffness mechanisms in a pin-jointed version of the same structure) (Guest and Hutchinson, 2003). The fully-patched design includes members on the periphery of every row in the Kagome plane, while the other has patches on alternate rows. The measurements are performed on panels laser cut from 304 stainless steel and from Ti–6Al–4V. Before embarking on calculations an eigenvalue analysis was used to establish the natural mode shapes. In the calculations, the bottom edge was completely clamped and the top edge was required to remain straight while being displaced in the vertical direction. The first modes (Fig. A.2), activated at the lowest load, are used to analyze the role of imperfections having relative amplitude, ξ: the ratio of the imperfection amplitude to member length. The load/deflection responses calculated for the *partially-patched* panels (Fig. A.3) and the deformed shapes (Fig. A.3) reveal that the responses become imperfection sensitive when $\xi \geqslant 10^{-3}$. Note that the peak load for the stainless steel structure involve plastic buckling at loads significantly above yield, while the Ti alloy panel fails by elastic buckling. The change from failure by plastic to elastic buckling is consistent

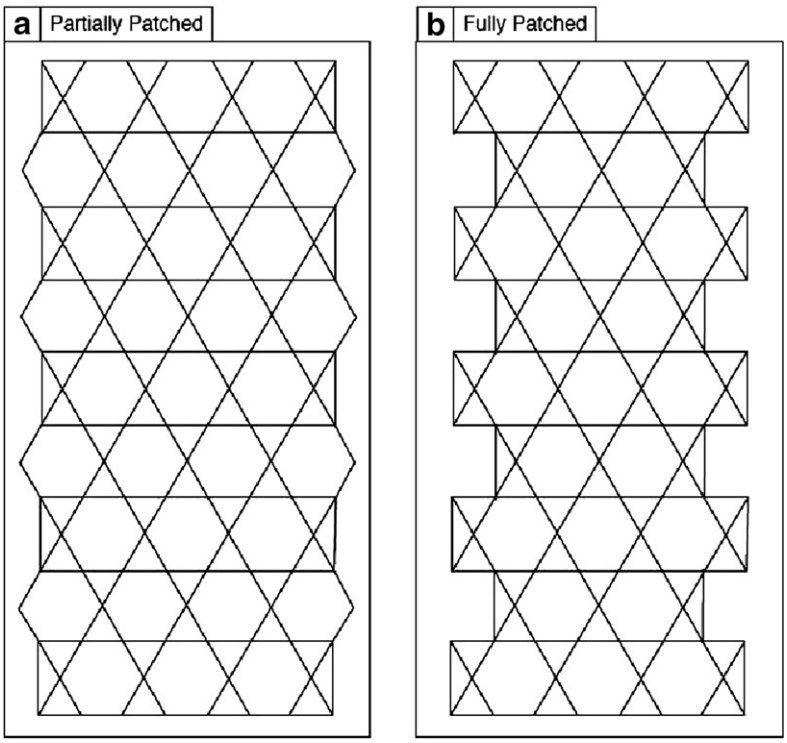

Fig. A1. Two different geometries of the Kagome plane: (a) partially patched; (b) fully patched.

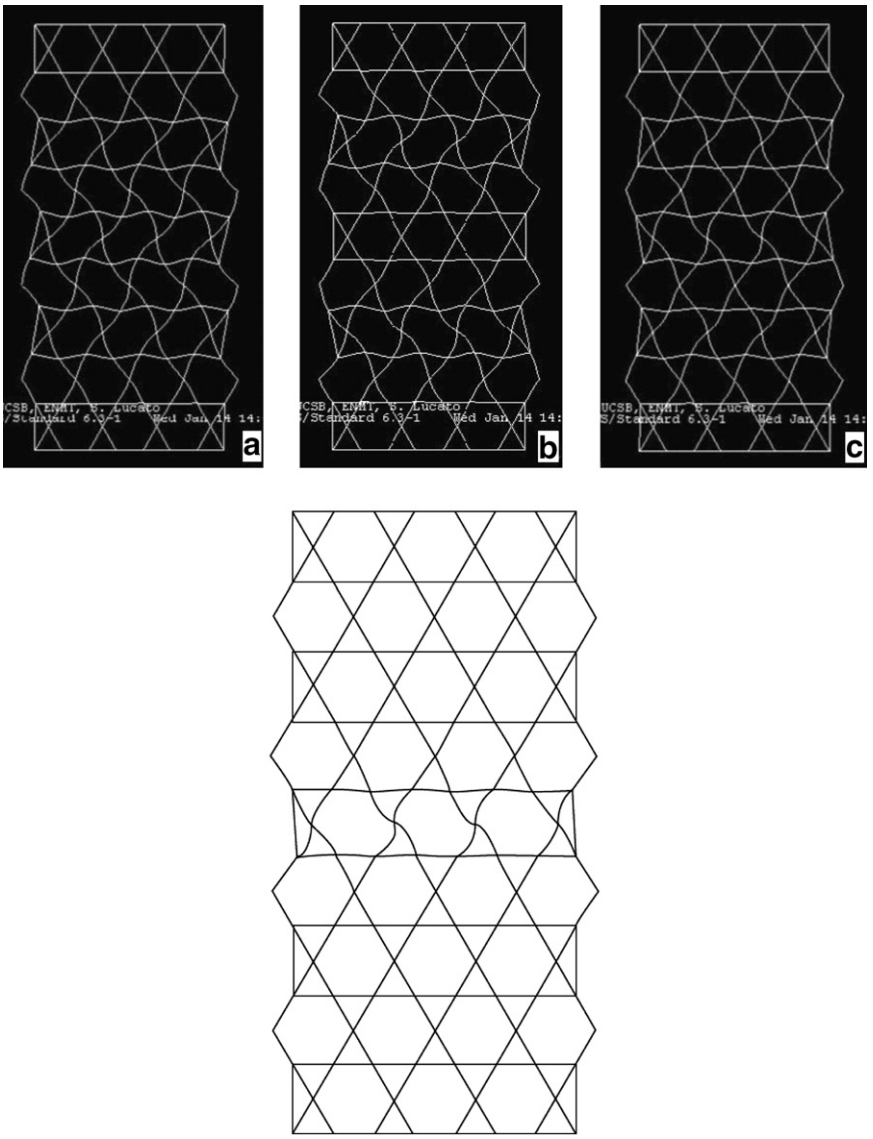

Fig. A.2. Shapes of the first three modes: (a) first; (b) second; (c) third, as well as the deformed shape near the load maximum.

with expectations (Hutchinson et al., 2003; dos Santos e Lucato et al., 2004). Prior to attainment of the load maximum, the central row of trusses rotate. This rotation triggers collapse of the un-patched rows in a pattern reminiscent of the mechanism that operates in the pin-jointed Kagome (Fig. A.4) (Symons et al., 2005a; Symons et al., 2005b). The corresponding results for the *fully-patched* designs (Fig. A.5) indicate that the load/deflection responses are much less imperfection sensitive and that the rotation-induced collapse mechanism is suppressed.

Compression tests were conducted by using thick glass constraining plates to eliminate out-of-plane displacements. To minimize frictional drag, the plates were separated by spacers incorporated at the bolted joints, 50 μm thicker than the specimen. The peak loads ascertained for a range of imperfection size (Fig. A.6) indicate that the Ti alloy structures fail by elastic buckling at a load, $P_{\max} = 5.2$ kN: while the steel structures failed by plastic buckling at $P_{\max} = 3.3$ kN. Note that the load capacities measured for both materials are within the calculated range assuming small imperfections, $\xi \leqslant 10^{-4}$ (Fig. A.6). This imperfection size corresponds to an actual amplitude of approximately 0.05 mm, similar to the dimensional tolerance for precision laser cutting systems (J. Furphy & Sons Pty Ltd.). *The important implication is that the imperfections*

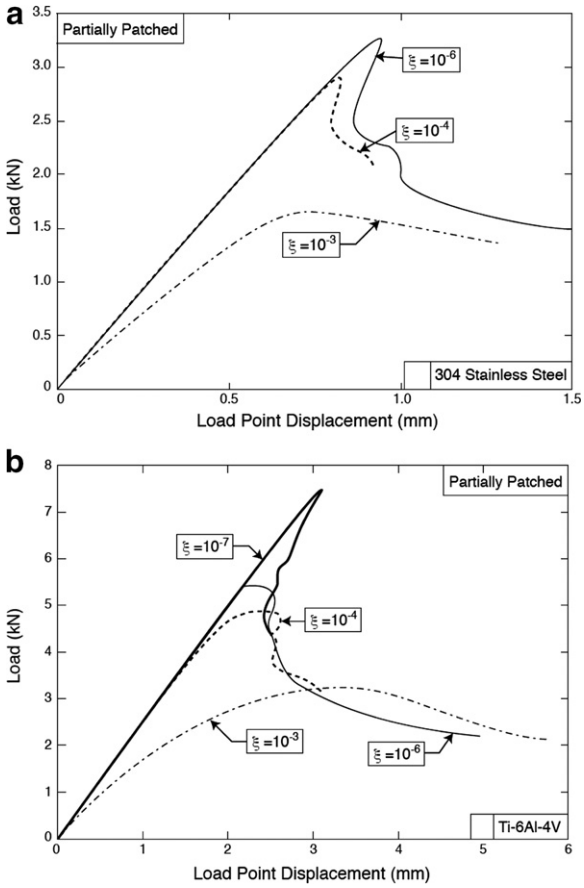

Fig. A.3. Load/displacement curves for the partially-patched panels for a range of imperfection amplitudes: (a) 304 stainless steel; (b) Ti–6Al–4V.

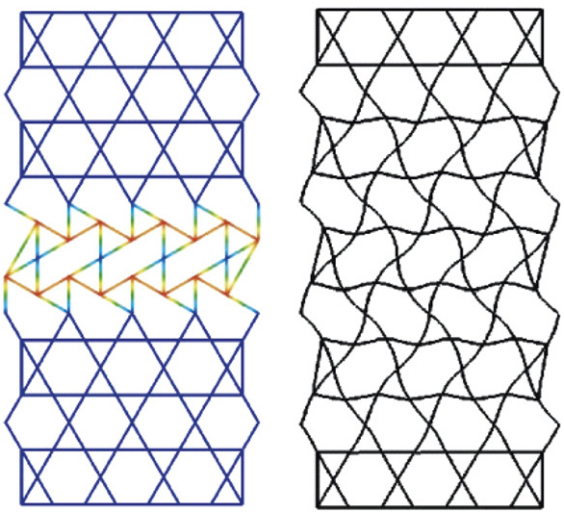

Fig. A.4. characteristic deformation pattern of truss rotation for pinned (left) and bonded joints.

caused by laser cutting are in a range where the imperfection sensitivity is minimal. A pursuant implication is that there is no particular load capacity detriment to using the partially patched design used in the present study (dos Santos e Lucato et al., 2004).

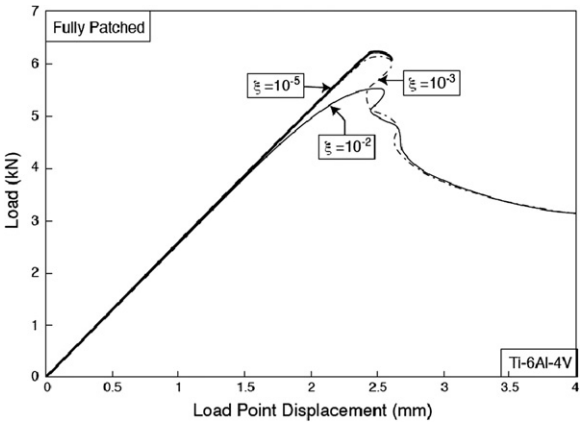

Fig. A.5. Load/displacement curves for fully patched Ti alloy panels for a range of imperfection amplitudes.

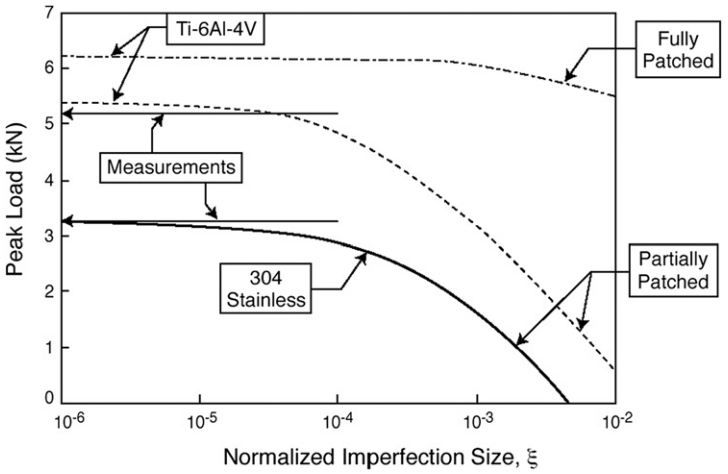

Fig. A.6. Trend in the peak load with imperfection amplitude for partially and fully-patched panels: stainless steel and Ti alloy. The measured peak loads are superposed.

Finally, images of specimens strained well beyond failure are summarized in Fig. A.7. At ~0.5% strain, the truss pairs near the right edge of row 4 distort and buckle, causing the adjacent nodes to rotate, and a truss pair near the right edge of row 5 to buckle. This failure differs from the finite element results, which predict symmetric collapse of row 5. This disparity is attributed to the slight loading asymmetry in the experiments.

Appendix B. Maximizing the twist (dos Santos e Lucato et al., 2004)

The objective is to actuate the structure so that the free edge twists but remains straight. For this purpose, n points are identified along the edge. The vertical displacement of each is controlled and maximized by selecting actuator strains for m independent actuators, where $m > n$. The redundancy among the actuators is used to optimize within the force capabilities of the actuators: a crucial requirement for *actuator-limited* structures. From analysis without passive loading, an n by m matrix, with rank n is constructed. A required twist can be achieved by specifying the n displacements for the control points, plus any values for the remaining m–n parameters. Express the control point displacements in terms of a single degree of freedom, ϕ, representing the amount of twisting:

$$v_i = \phi \bar{v}_i \tag{B.1}$$

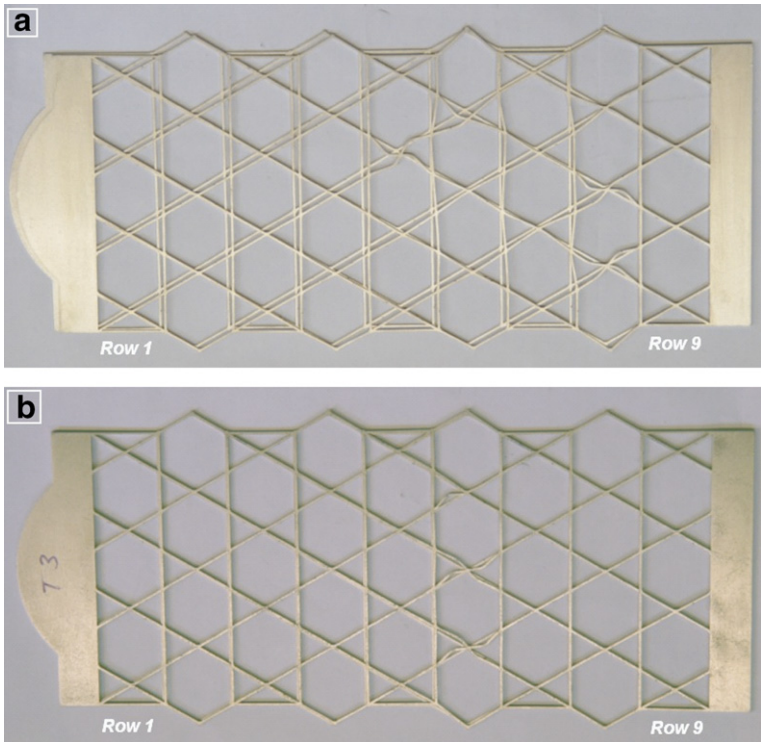

Fig. A.7. Deformed partially patched specimens tested in compression: (a) stainless steel and (b) Ti alloy.

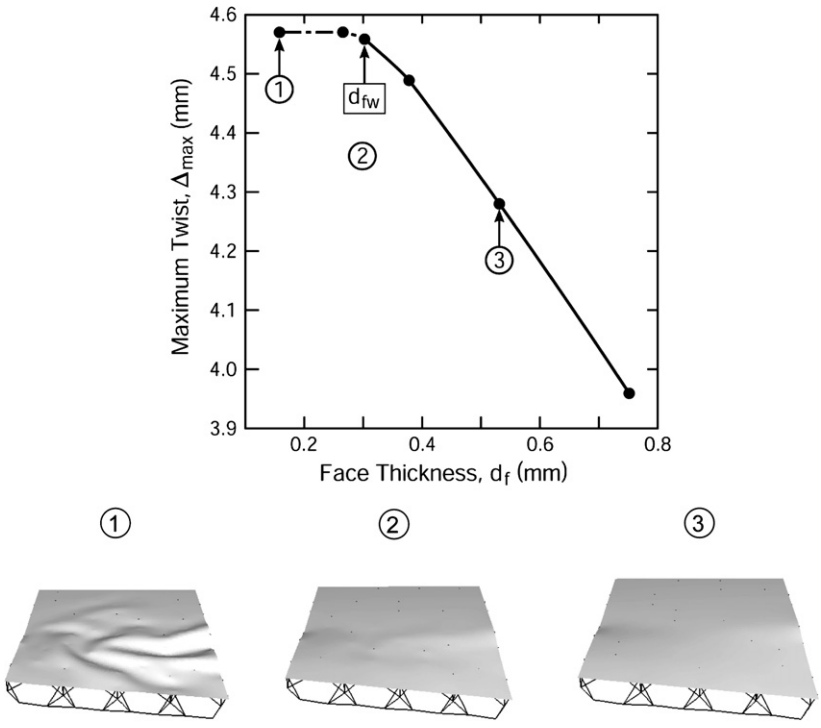

Fig. B.1. The maximum twist displacement realizable for different face thickness and the wrinkling patterns of the solid face sheets.

where $\bar{v}_i$ are the displacements of the control points for unit value of ϕ. Finally, maximize ϕ subject to minimum and maximum constraints on the actuator forces. This is a linear programming problem to find the m–n coordinates of the displacements. Once solved, the resulting ϕ are used to compute the actuator strains that produce the maximum possible twist within the actuator force constraints.

Appendix C. Experimental validation of face wrinkling

A series of experiments has been conducted using the demonstration structure with a Kagome plane and a core made from 304 stainless steel and a face made from a high strength Al alloy. To emphasize face wrinkling, this structure is tested with the linear actuator array. To guide the experiments, numerical simulations have been conducted for an actuator load capacity, $X_{\mathrm{Act}} = 40$ N. The realizable twisting is plotted in Fig. B.1. The twisted configurations are also indicated in the figure. Note that, for this case, the simulations predict, $d_{\mathrm{fw}} = 0.30$ mm.

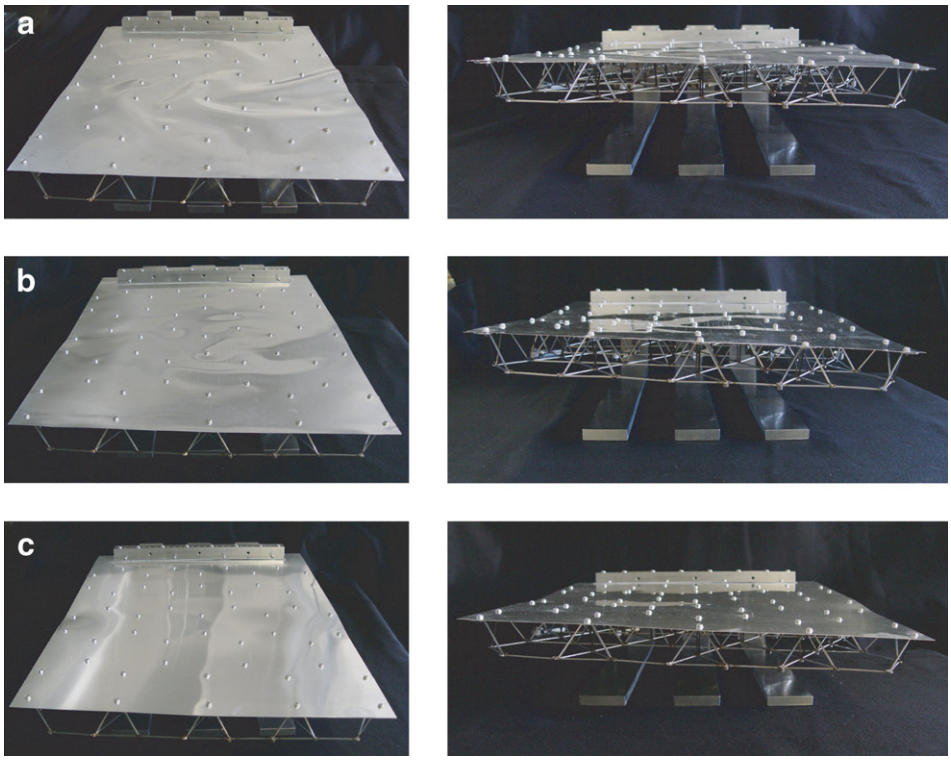

Fig. B.2. Face wrinkling suppressed by increasing the face-sheet thickness: (a) $d_{\mathrm{f}} = 0.15$ mm, below critical face-sheet thickness d_{fw}, dramatic face wrinkling observed; (b) $d_{\mathrm{f}} = 0.30$ mm, critical face-sheet thickness d_{fw}, face distortion observed; (c) $d_{\mathrm{f}} = 0.53$ mm, above critical face-sheet thickness d_{fw}, smooth twist without face wrinkling.

Table 5
Comparison of the achieved twist displacements between numerical simulation and test. Δ_{up} is the upward displacement of one corner and Δ_{down} the downward displacement of the other

Face-sheet (mm)	Thickness twist at the edge			
	FEA		Test	
	Δ_{down}	Δ_{up}	Δ_{down}	Δ_{up}
0.15	−1.41	5.76	−2.3	6.2
0.30	−4.56	4.56	−4.8	5.5
0.53	−4.35	4.28	−4.7	5.3

Based on commercial availability, aluminum sheets with three different thicknesses were chosen that bound d_{fw}: these were, $d_f = 0.15$, 0.30, 0.53 mm. Turnbuckles were used to impose the displacements indicated in Table 1, assuring that the loads never exceed 40 N. Images of the panels at the maximum twist are shown in Fig. B.2. Consistent with the calculations, the result for the thinnest panel ($d_f/d_{fw} = 0.5$) reveals dramatic wrinkling. Moreover, the wrinkling pattern is remarkably similar to that found in the calculations (Fig. B.1). Also in accordance with the calculations, the assembly with the thickest face ($d_f/d_{fw} = 1.8$) displayed a smooth twist. The intermediate panel ($d_f/d_{fw} = 1$) did not wrinkle but exhibited some face distortion. All of the twist displacements are comparable to the calculated values (Table 5). *We conclude that the numerical procedure captures the incidence of face wrinkling with high fidelity*.

References

Ashby et al., 2000. Metal Foams: A Design Guide. Butterworth-Heinemann, Boston.

Christensen, R.M., 2000. Mechanics of cellular and other low-density materials. Int. J. Solids Struct. 37, 93–104.

dos Santos e Lucato, S.L., Evans, A.G., 2006. The load capacity of a Kagome based high authority shape morphing structure. J. Appl. Mech. 14, 128–133.

dos Santos e Lucato, S.L., Wang, J., Maxwell, P., McMeeking, R.M., Evans, A.G., 2004. Design and demonstration of a high authority shape morphing structure. Int. J. Solids Struct. 41, 3521–3543.

dos Santos e Lucato, S.L., McMeeking, R.M., Evans, A.G., 2005. Actuator placement optimization in a Kagome based high authority shape morphing structure. Smart Mater. Struct. 14, 869–875.

Guest, S.D., Hutchinson, J.W., 2003. On the determinacy of repetitive structures. J. Mech. Phys. Solids 51, 383–391.

Hutchinson, R.G., Wicks, N., Evans, A.G., Fleck, N.A., Hutchinson, J.W., 2003. Kagome plate structures for actuation. Int. J. Solids Struct. 40, 6969–6980.

Hyun, S., Torquato, S., 2002. Optimal and manufacturable two-dimensional Kagome-like cellular solids. J. Mater. Res. 17, 137–144.

J. Furphy and Sons Pty Ltd. Laser Cutting Technology. Available from: <http://www.furphys.com.au/lasertech.html>.

Lu, T.J., Hutchinson, J.W., Evans, A.G., 2001. Optimal design of a flexural actuator. J. Mech. Phys. Solids. 49, 2071–2093.

Symons, D.D., Hutchinson, R.G., Fleck, N.A., 2005a. Actuation of the Kagome double layer grid. Part 1 prediction of performance of the perfect structure. J. Mech. Phys. Solids 53, 1855–1874.

Symons, D.D., Shieh, J., Fleck, N.A., 2005b. Actuation of the Kagome double layer grid. Part 2: effect of imperfections on the measured and predicted actuation stiffness. J. Mech. Phys. Solids 53, 1875–1891.

Wicks, N., 2003. Optimization and actuation of truss structures. Ph.D Thesis, Engineering Sciences, Harvard University, Cambridge, Massachusetts.

Wicks, N., Hutchinson, J.W., 2001. Optimal truss plates. Int. J. Solids Struct. 38, 5165–5183.

Mathematica 5.0, 2003. Wolfram Research, Champaign, IL, USA. Available from: <www.wolfram.com>.